Research Article | Vol. 27, No. 18 | 2 Sep 2019 | OPTICS EXPRESS 25064
Optics EXPRESS

Time resolved Brillouin fiber-spectrometer

SALVATORE LA CAVERA III,* FERNANDO PÉREZ-COTA, RAFAEL FUENTES-DOMÍNGUEZ, RICHARD J. SMITH, AND MATT CLARK

Optics and Photonics Group, Faculty of Engineering, University of Nottingham, University Park, Nottingham, NG7 2RD, UK
*salvatore.lacaveraiii@nottingham.ac.uk

Abstract: This report introduces a novel time resolved Brillouin spectrometer, consisting of an opto-acoustic transducer which resides on the tip of a single-mode optical fiber of arbitrary length with 125 μm outer diameter and 5 μm sensing diameter. Demonstrated here are proof of concept spectroscopic measurements – shifts in Brillouin frequency – with sensitivities of 41±3 MHz/%wt and 2.5±0.6 MHz/°C for changes in water-salinity and water-temperature, respectively, and an interpolated frequency resolution of 9±2 MHz. The technique benefits from low-cost raw materials, scalable fabrication, scalable pixel density, easy alignment, and data acquisition speeds down to 0.4 s: traits which make this compatible with *in vivo* applications.

1. Introduction

Brillouin spectroscopy is a well-established optical technique for characterizing and imaging mechanical properties of various photoelastic media [1–3]. The collection of techniques has long relied on non-trivial free-space optical arrangements and exclusively *in vitro* instrumentation to couple light into and back from the sample. There have been previous successful implementations of *in vivo* Brillouin spectroscopy [3], but expanding the range of the free-space technique is limited by the penetration depth of light in biological tissue (~ 1 cm in the NIR spectrum [4]).

In the field of photoacoustics, there has been a flurry of development in optical fiber-based ultrasonic transmitters (multi-mode) and receivers (single-mode), which, when combined, create a powerful endoscopic tool for *in vivo* tissue imaging with ~ 20 MHz ultrasound [5]. A similar dual-fiber (both single-mode) concept has also been implemented for performing spontaneous Brillouin spectroscopy in the GHz-range on liquid samples [6]. This technique is ultimately challenging with a single-mode fiber since it relies on an inherently inefficient incoherent scattering process and contends with strong background signals from the glass of the fiber. In order to combat these difficulties, the technique is reliant on two separate fibers (transmitter and receiver) terminated by a graded index lens (~ 15 times greater diameter than the fiber), which limits the pixel-density scalability of the technique in the context of future imaging. Otherwise, the role of optical fibers in GHz-frequency ultrasonic applications has mainly been one of collecting scattered light, creating a confocal pinhole, or as a way to simplify alignment [7].

We present in this report a proof of concept for a novel *phonon probe*, which permits time resolved Brillouin spectroscopic measurements to be made from the tip of a single-mode optical fiber without the need for a lens. Two main criteria drove the design: (1) that there is sufficient generation of ultrasound from the tip of the fiber, and, (2) that the back-scattered probe light can be efficiently re-coupled into the same fiber. The sensitivity of the device, and other Brillouin techniques in general, derives from Brillouin light scattering, whereby light is inelastically scattered by phonons [8]. In time resolved Brillouin scattering (TRBS), the interference of the scattered light and a reference beam (reflected from the fiber-tip) produces a modulation in optical intensity which occurs at a characteristic Brillouin frequency:

$$f_B = \frac{2nv}{\lambda_{probe}} \tag{1}$$

#369096 https://doi.org/10.1364/OE.27.025064
Journal © 2019 Received 3 Jun 2019; accepted 31 Jul 2019; published 20 Aug 2019

Optics EXPRESS

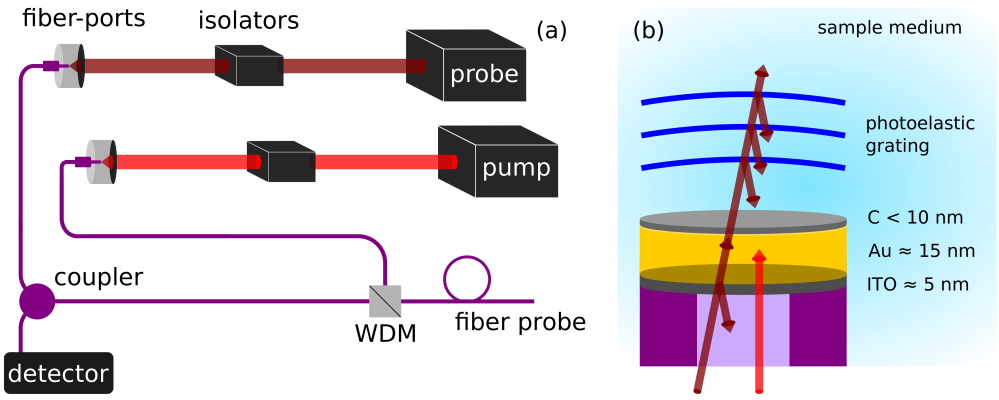

Fig. 1. (a) Diagram of the optical system designed and used for the single-fiber Brillouin spectrometer. (b) The device architecture consists of a 125 μm outer diameter (cladding), 5 μm sensing diameter (core), and adhesion (ITO), generation (Au), and hydrophobic (C) layers. Visualization of Brillouin scattering: light reflected by the fiber-transducer interface interferes with the light scattered by periodic changes in the refractive index of the external medium (water).

(for normal incidence) where n is the refractive index of the medium, v the sound velocity, and λ_{probe} the wavelength of the probing light [9]. A system such as the *phonon microscope* capitalizes on this mechanism to acoustically image living cells in 3D through the use of an opto-acoustic transducer to thermo-elastically generate coherent phonons [10, 11]. By coherently stimulating phonons (while using a time resolved detection scheme), the efficiency of the detected scattering process can increase by ~ 6 orders of magnitude compared with spontaneous scattering, providing a more effective way to spatially and temporally resolve the phonons.

2. Method

Similar to the phonon microscope, the phonon probe utilizes an optical pump-probe configuration to acquire TRBS signals (shown in Fig. 1(a)). Two tunable Ti:Sapphire lasers, with 100 fs pulse widths and 80 MHz repetition rates, were used for the thermoelastic-generation (pump) and detection (probe) of coherent GHz-frequency phonons [12]. Temporally resolving the signals was achieved using asynchronous optical sampling [13], whereby the repetition rate of the slave is increased by 10 kHz with respect to the 80 MHz master, corresponding to full reconstruction of the 12.5 ns signal every 100 μs.

Typically, pump-probe imaging and spectroscopy experiments use high numerical aperture (NA) objective lenses to reduce the laser spot-sizes, which increases the lateral resolution of the imaging system and the intensity of the optical fields. The latter dictates the amplitude of the phonon field, the intensity of the scattering probe light, and consequently the overall signal to noise ratio (SNR). The optical design for an all-fiber variant of a pump-probe system was centered around maximizing SNR, given that the laser spot-sizes were to be dictated by the 5 μm diameter core of a single-mode optical fiber (125 μm diameter cladding). The following series of elements were selected to reduce noise and optimize fiber-coupling efficiency (see Fig. 1(a)): Faraday isolators, a fiber-coupler, and a wavelength division multiplexer (WDM). Pump and probe wavelengths were selected as 730 and 780 nm, respectively, based on the dichroic edge of the WDM and the single-mode cut-off wavelength for co-propagating in a single fiber. The transducer was fabricated onto the cleaved fiber-tip by DC magnetron sputtering and carbon-rod evaporation with the following layer design: ≈ 5 nm adhesion layer of indium tin oxide (ITO), 15

Optics EXPRESS

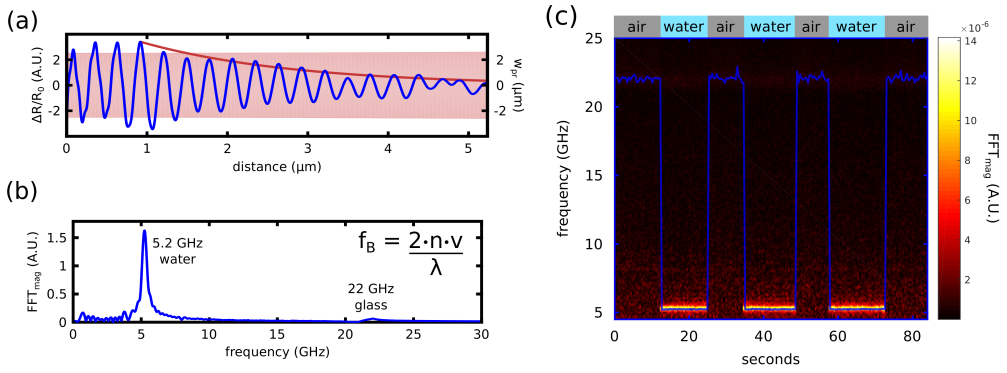

Fig. 2. (a) Time resolved signal (blue line) from Brillouin scattering (in water). The dark red line represents the acoustic attenuation in water taken from literature [15], which matches the decay of the signal. Light red shading shows the divergence of the probe spot (w_{pr}). (b) Fast Fourier transform (FFT) of the time trace reveals Brillouin frequencies of 5.235±0.004 GHz (water) and 22.00±0.07 GHz (glass). (c) FFT magnitude color map, overlaid by the frequency at which the maximum magnitude occurs, as functions of experiment time. Probe-dipping in and out of water occurred every ≈ 10 s, as shown by the sharp transitions between 5.24±0.02 GHz (water) and 22.1±0.2 GHz (glass of fiber-core when tip is in air).

nm of gold for generation, and a thin layer of graphite for hydrophobicity (Fig. 1(b)). An example TRBS signal and corresponding Brillouin spectrum for water are presented in Figs. 2(a)-(b).

3. Results

Initially testing the performance of the probe took place by dipping the fiber-tip in and out of deionized water. The amplified and low-pass filtered output of the photodiode was visualized on a digital oscilloscope where the average of 1000 time traces was acquired for each measurement count; at this averaging rate, a count was acquired every ≈ 0.4 s. Data were acquired at this rate over the course of roughly 90 s, while the tip was made to transition from water to air every 10 s. Raw time trace data were processed post-experiment, following the protocol outlined in [14], and the corresponding frequency spectra were attained by fast Fourier transform (FFT). Fig. 2(c) shows the evolution of the Brillouin spectra for this set of measurements. From the color map of the FFT magnitude, which is a function of frequency and time, bright bands can be seen when the tip is immersed in water, as confirmed by the 5.24±0.02 GHz Brillouin frequency. This band abruptly disappears upon withdrawal of the probe from the water. A dimmer frequency band at 22.1±0.2 GHz persists throughout all measurements, which is the probe detecting itself, i.e. the Brillouin oscillations counter-propagating in the glass of the optical fiber. The blue curve tracks the frequency at which the maximum FFT amplitude occurs as a function of the experimental clock (f_B). As the tip transitions from water to air, there does not appear to be any residual water droplet on the outer hydrophobic layer, and this transition in frequency occurs within the time-span of one count (< 0.4 s).

In order to exhibit the sensitivity of the phonon probe in other liquids, Brillouin spectroscopic measurements were made in a range of static and dynamic solutions. Initially, a cocktail of one part water and one part glycerol was prepared, and the layers were allowed to settle and differentiate. The z-position of the probe-tip was controlled by micrometer, which facilitated a controlled immersion through the solution in the following sequence: air, water, glycerol, water, and air. Over the course of ≈ 24 minutes, time trace data were acquired with a higher

Optics EXPRESS

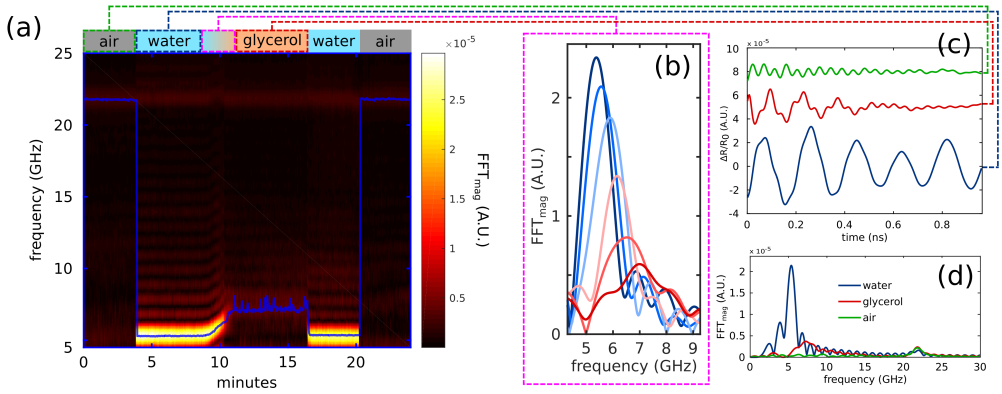

Fig. 3. (a) Spectroscopy in air, water, glycerol, water, and air. (b) Shifts in Brillouin frequency and spectral broadening as the probe-tip slowly approached glycerol. (c) Example TRBS signals averaged from the air, glycerol, and water layers. (d) Corresponding frequency spectra for traces in (c), revealing maxima at 5.24±0.08, 7.20±0.28, and 21.80±0.04 GHz for water, glycerol, and glass respectively.

averaging rate of 10,000 averages per measurement count (≈ 3 s per count). The combined FFT magnitude map and Brillouin spectra, versus experiment time, is presented in Fig. 3(a), along with supplemental signals and spectra in Figs. 3(b)-(d). The signals in each material were processed from the time domain to the frequency domain using the same set of parameters, except for the polynomial fit order used to remove the background thermal decay. The transition from water to glycerol is clearly visible in Fig. 3(b); as the acoustic attenuation becomes more fierce in the viscous glycerol, the acoustic amplitude falls and the spectral width broadens. In addition, the central frequency peak is located at 7.20±0.28 GHz which is consistent with glycerol refractive index and sound velocity data from literature [16, 17].

Additional experiments were carried out to demonstrate the probe's ability to detect changes in the state of a solution. The well known variations in the refractive index and sound velocity of water, as functions of solute concentration and temperature, were used as case studies. In order to detect changes in the concentration of a solution, the device was dipped in a beaker of deionized water; during TRBS data acquisition, salt solution was added every two minutes such that the overall concentration increased in ≈ 1-2%wt steps. Fig. 4(a) shows the corresponding shifts in Brillouin frequency (f_B) as the water becomes increasingly concentrated with salt. Refractive index and sound velocity data, as functions of salt concentration, were found in literature [18, 19] and used to formulate a theoretical Brillouin frequency (Eq. (1)) versus salt concentration analytical model ($f_B(C)$). Calibrated experimental Brillouin frequency peaks (discussed later) were input to the model, and concentrations at which the experimental and theoretical frequencies match provide a measure of the local salt concentration in the solution (C_{f_B}), which corroborate the approximate experimental concentration (C_{exp}). From these measurements, an estimation of the probe's sensitivity to salt concentration can be extracted, and was calculated to be $\Delta f_B/\Delta C$ = 41±3 MHz/%wt. The stars on each curve represent additional averaging within the respective step in concentration; the sizing of the averaging bins determines the precision with which a Brillouin frequency step can be resolved from neighboring steps. In order to probe these resolution limits, a subsequent experiment was performed where each salt concentration increment was halved with respect to the preceding increment. Fig. 4(b) reveals the frequency steps between the first four changes in salt concentration: 40, 19, and 9±2 MHz. It is important to note that the fundamental frequency resolution of the system is set by the repetition rate of the detection laser, 80 MHz.

Optics EXPRESS

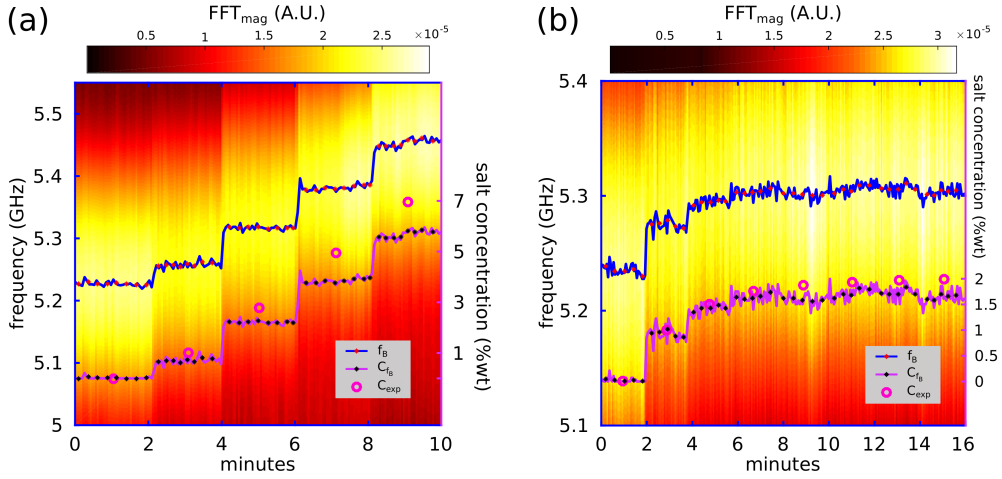

Fig. 4. (a) Brillouin frequency shifts as water-salinity increases (f_B). Salinity measurements made by the probe (C_{f_B}) agree with the approximate experimental concentration added (C_{exp}). Stars represent post-processing averaging in each step. (b) Decreasing salt concentrations were added to quantify the effective frequency resolution of the probe given the optical system.

However, since the signal of interest has a wider bandwidth than the 80 MHz steps in frequency, zero-padding can be used to *interpolate* the 80 MHz-discretized data. Consequently, there exists a trade-off between experiment time and processed frequency resolution. If detecting small shifts in a sample's properties is desired, two neighboring frequency peaks can be resolved if sufficient time is taken to increase the number of averages per measurement.

For the case of temperature-sensitivity, the probe was immersed in a beaker of deionized water, as were the leads of a K-type thermocouple which had been calibrated at the boiling point of water. A hot-plate beneath the beaker was varied over two hours while both TRBS and thermocouple data were simultaneously acquired. The blue curve (f_B) in Fig. 5(a) represents the Brillouin frequency shift as the hot-plate undergoes heating and cooling, following the first 20 minutes at room temperature (RT$\approx$ 20°C). Experimental Brillouin frequencies were combined with thermo-optic and thermo-acoustic constants (water) from literature [20, 21] to produce an experimental measurement of the local water temperature (T_{f_B}). All preceding measurements of the Brillouin frequency of water (at RT and 0%wt salt), ~ 5.2 GHz, are offset from the theoretical value ~ 5.1 GHz, which we believe to be explainable in the context of heating by the transducer. The offset between the theoretical and RT Brillouin frequencies would then represent the heating contribution by the probe itself, and was determined with the experimental model to be $\approx$ 60°C. Finite element (FEM) software (COMSOL) was utilized to simulate the steady-state heat rise in the $5 \times 5 \times 5$ μm volume of water surrounding the tip of the fiber-core (see Fig. 5(b)). For the roughly 3 mW of total optical average power absorbed by the transducer, the simulated results indicate an average temperature rise of $\approx$ 55°C in the volume of interest, which corroborates the temperature rise measured by the probe. After calibrating for this bias, temperatures matched between the literature-model and experiment (T_{f_B}) can be seen to mirror the values and trends of the thermocouple data (T_{TC}). The device's sensitivity to temperature was measured to be $\Delta f_B/\Delta T$ = 2.5±0.6 MHz/°C, which is in agreement with the $f_B(T)$ slope of the literature-based model.

Optics EXPRESS

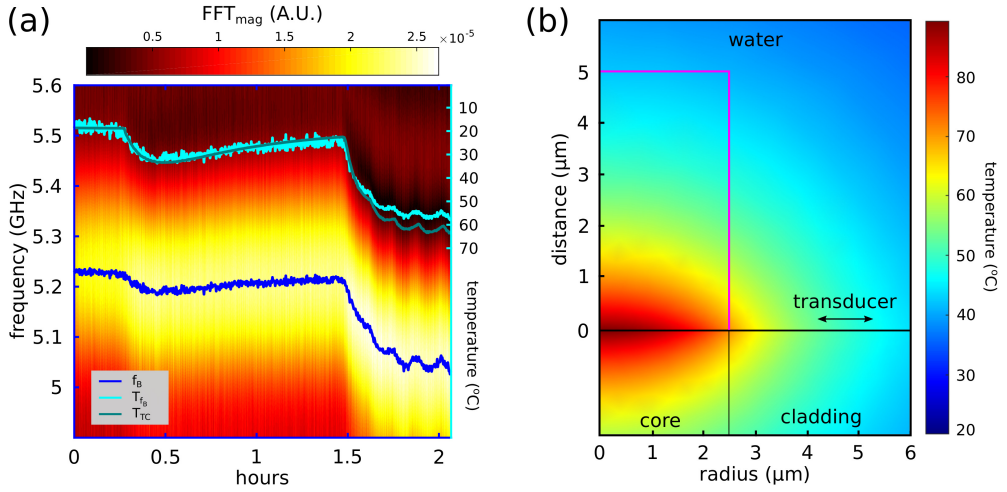

Fig. 5. (a) Brillouin frequency shifts caused by fluctuations in water temperature, which follow the trend in thermocouple data (T_{TC}). Overlaid is the reconstruction of the experimental frequency data into temperature readings (T_{f_B}). (b) FEM modeled (axially symmetric) temperature rise in the $5 \times 5 \times 5$ μm volume of water surrounding the tip of the fiber-core (pink outlined region).

4. Discussion

In this all-fiber approach to performing pump-probe Brillouin spectroscopic measurements, once light has been optimally coupled to fiber, the system is always "perfectly" aligned and overlapped (with respect to the pump and probe spots). What's more, compared to more complicated conventional pump-probe spectroscopy and Brillouin spectroscopy set ups, there are far fewer aberrating optical elements and other mechanisms of loss. The primary effects to consider are those of dispersion and leakage into the cladding, which did not produce noticeable penalties in this experiment. With respect to optimizing the optical system, there are various improvements which could be made, the most obvious of which is the choice in probe coupler used before the WDM. The probe beam suffers a loss of 3 dB upon input and another 3 dB at detection. If a fiber optic circulator was used instead, this could be reduced to < 1 dB overall insertion loss. In contrast with high NA objective experiments, the lateral resolution of the fiber probe is the core diameter of 5 μm, which could be improved by tapering the fiber-tip. Despite having lower lateral resolution, the axial resolution of the probe, in theory, is sub-optical diffraction limit, just as with the phonon microscope [11]. In practice these or similar resolutions can be achieved for imaging and profilometry applications by controlling the location of the probe-tip using high resolution positioners.

Realizing the potential of the phonon probe as an *in vivo* instrument will require careful consideration of a sample's exposure to heating and fs-pulse width radiation. With regards to the transducer's 60°C heating of water, simply reducing the total absorbed average power by a factor of two would reduce the temperature rise by nearly 30°C according to FEM model. Similar reduced power densities of NIR fs-radiation have been reported as survivable for Chinese hamster ovary cells [22]. Additionally, the probe could be supplemented with a thin thermally insulating coating or a more thermally conductive fiber material, such as sapphire [11, 23]. Currently, the light transmitted by the device exceeds the maximum permissible exposure (MPE) for direct ocular exposure by a factor of 2; again, if the total average power is halved, the MPE would be safely met. There exists a compromise between heating/exposure mitigation and SNR

which could be partially compensated for by using the aforementioned circulator, or at worst by increasing data-averaging over longer time periods.

With our current thin-film deposition machinery there is enough space to fit hundreds of thousands of 125 μm diameter by one meter fibers. In practice this would be time-consuming to prepare (by hand), but the prospect for mass-production of the devices is not lost. Furthermore, the cost per-fiber is on the order of $5 per meter, and would be marginally more expensive when including overhead and sputtering material.

The phonon microscope is capable of imaging polymer structures and cellular media, *in vitro*, and does so by performing a spectroscopic measurement (Brillouin frequency and sound velocity) at each pixel in the scan-area to render an elastic-image. Compared to the phonon microscope, the phonon probe presented here, has proven that a similar quality of single-point spectroscopic measurements can be attained. The current iteration of the device presented in this report could already be capable of performing *in situ* spectroscopy measurements in industrial liquid monitoring applications where traditional sensors cannot fit, or where access is limited. Similar measurements could also be performed *in vivo* through the tip of a needle or the channel of an endoscope – e.g. as an alternative to biopsies and tissue diagnostics, or as a surgical guide in epidural procedures – however, more investigation is needed to find compatible tissue and bio-liquids. In theory, N-number of fiber probes can be bundled to create an N-pixel phonon imaging tool. Recent advances in *in vitro* Brillouin imaging and phonon microscopy have allowed imaging, and even characterization, of elastic properties in colorectal cancer cells [24] and acanthamoeba castellani cells [25]. If a device such as the phonon endoscope can be fully realized in an imaging context, there would be great potential to elastically map tumorous or infectious agents in an *in vivo* environment.

5. Conclusion

In conclusion, we have designed and implemented a novel tool, and with it have demonstrated for the first time that time resolved Brillouin spectroscopic measurements can be made from the tip of a single-mode optical fiber without a lens. Proof of concept measurements were made in a range of water-solutions and glycerol with data acquisition speeds down to 0.4 s. Through post-processing and data-averaging, the device is capable of resolving sub-repetition rate interpolated shifts in Brillouin frequency. There are additional thermal and optical accommodations required to enable *in vivo* operation, however, most of these optimizations are within the capabilities of the current experiment. A single-fiber device for point-by-point measurements can be easily integrated to the channel of an endoscope, the bore of a needle, or any space greater than 125 μm. Perhaps one of the more promising aspects of the phonon probe, is that its simple and compact design can be easily scaled to any arbitrary number of fibers in a bundle, which bodes well for multi-pixel acoustic imaging and endoscopic microscopy in biomedical applications.

Funding

The Engineering and Physical Sciences Research Council (EP/K021877/1, EP/G061661/1, EP/L015587/1); The Royal Academy of Engineering Research Fellowship (RF_201718_17144).

Acknowledgements

SLC would like to acknowledge Rolls-Royce plc, YouCare Technology Co., Ltd, and NDEvR (RCNDE) for the support of his studentship, and Sidahmed Abayzeed for his helpful discussions.

References

1. G. Scarcelli and S. H. Yun, "Confocal Brillouin microscopy for three-dimensional mechanical imaging," Nat. Photonics **2**, 39–43 (2008).

Optics EXPRESS

2. T. Dehoux and B. Audoin, "Non-invasive optoacoustic probing of the density and stiffness of single biological cells," J. Appl. Phys. **112**, 124702 (2012).
3. G. Scarcelli and S. H. Yun, "In vivo Brillouin optical microscopy of the human eye," Opt. Express **20**, 9197 (2012).
4. W. F. Cheong, S. A. Prahl, and A. J. Welch, "A review of the optical properties of biological tissues," IEEE J. Quantum Electron. **26**, 2166–2185 (1990).
5. M. C. Finlay, C. A. Mosse, R. J. Colchester, S. Noimark, E. Z. Zhang, S. Ourselin, P. C. Beard, R. J. Schilling, I. P. Parkin, I. Papakonstantinou, and A. E. Desjardins, "Through-needle all-optical ultrasound imaging in vivo: a preclinical swine study," Light. Sci. Appl. **6**, e17103 (2017).
6. I. V. Kabakova, Y. Xiang, C. Paterson, and P. Török, "Fiber-integrated Brillouin microspectroscopy: Towards Brillouin endoscopy," J. Innov. Opt. Heal. Sci. **10**, 1742002 (2017).
7. G. Pakulski and F. Holuj, "Fiber-optics Brillouin scattering spectrometer," Rev. Sci. Instrum. **61**, 1390–1394 (1990).
8. L. Brillouin, "Diffusion de la lumière et des rayons X par un corps transparent homogène: Influence de l'agitation thermique," Ann. Phys. **9**, 88–122 (1922).
9. C. Thomsen, J. Strait, Z. Vardeny, H. J. Maris, J. Tauc, and J. J. Hauser, "Coherent phonon generation and detection by picosecond light pulses," Phys. Rev. Lett. **53**, 989–992 (1984).
10. F. Pérez-Cota, R. J. Smith, E. Moradi, L. Marques, K. F. Webb, and M. Clark, "Thin-film optoacoustic transducers for subcellular Brillouin oscillation imaging of individual biological cells," Appl. Opt. **54**, 8388 (2015).
11. F. Pérez-Cota, R. J. Smith, E. Moradi, L. Marques, K. F. Webb, and M. Clark, "High resolution 3D imaging of living cells with sub-optical wavelength phonons," Sci. Rep. **6**, 39326 (2016).
12. R. Fuentes-Domínguez, F. Pérez-Cota, S. Naznin, R. J. Smith, and M. Clark, "Super-resolution imaging using nano-bells," Sci. Rep. **8**, 16373 (2018).
13. P. A. Elzinga, F. E. Lytle, Y. Jian, G. B. King, and N. M. Laurendeau, "Pump/probe spectroscopy by asynchronous optical sampling," Appl. Spectrosc. **41**, 2–4 (1987).
14. R. J. Smith, F. P. Cota, L. Marques, X. Chen, A. Arca, K. Webb, J. Aylott, M. G. Somekh, and M. Clark, "Optically excited nanoscale ultrasonic transducers," J. Acoust. Soc. Am. **137**, 219–227 (2015).
15. F. Yang, T. Atay, C. H. Dang, T. J. Grimsley, S. Che, J. Ma, Q. Zhang, A. V. Nurmikko, and H. J. Maris, "Study of phonon propagation in water using picosecond ultrasonics," J. Phys. Conf. Ser. **92**, 012024 (2007).
16. J. Rheims, J. Köser, and T. Wriedt, "Refractive-index measurements in the near-IR using an Abbe refractometer," Meas. Sci. Technol. **8**, 601–605 (1997).
17. F. A. A. Fergusson, E. W. Guptill, and A. D. MacDonald, "Velocity of sound in glycerol," J. Acoust. Soc. Am. **26**, 67–69 (1954).
18. X. Quan and E. S. Fry, "Empirical equation for the index of refraction of seawater," Appl. Opt. **34**, 3477–3480 (1995).
19. K. V. Mackenzie, "Discussion of sea water sound-speed determinations," J. Acoust. Soc. Am. **70**, 801–806 (1981).
20. A. N. Bashkatov and E. A. Genina, "Water refractive index in dependence on temperature and wavelength: a simple approximation," in *Saratov Fall Meeting 2002: Optical Technologies in Biophysics and Medicine IV,* vol. 5068 (International Society for Optics and Photonics, 2003), pp. 393–395.
21. F. Yang, T. J. Grimsley, S. Che, G. A. Antonelli, H. J. Maris, and A. V. Nurmikko, "Picosecond ultrasonic experiments with water and its application to the measurement of nanostructures," J. Appl. Phys. **107**, 103537 (2010).
22. K. König, P. T. C. So, W. W. Mantulin, and E. Gratton, "Cellular response to near-infrared femtosecond laser pulses in two-photon microscopes," Opt. Lett. **22**, 135–136 (1997).
23. C. Hill, D. Homa, Z. Yu, Y. Cheng, B. Liu, A. Wang, and G. Pickrell, "Single mode air-clad single crystal sapphire optical fiber," Appl. Sci. **7**, 473 (2017).
24. J. Margueritat, A. Virgone-Carlotta, S. Monnier, H. Delanoë-Ayari, H. C. Mertani, A. Berthelot, Q. Martinet, X. Dagany, C. Rivière, J.-P. Rieu, and T. Dehoux, "High-frequency mechanical properties of tumors measured by Brillouin light scattering," Phys. Rev. Lett. **122** (2019).
25. F. Pérez-Cota, R. J. Smith, H. M. Elsheikha, and M. Clark, "New insights into the mechanical properties of Acanthamoeba castellanii cysts as revealed by phonon microscopy," Biomed. Opt. Express **10**, 2399–2408 (2019).